Electron beam monitoring of a modified conventional medical accelerator with a portable current transformer system traceable to primary electrical standards

Renaud, James; Muir, Bryan Richard; Williams, Andrew; McEwen, Malcolm

Publisher's version / Version de l'éditeur:

https://doi.org/10.1002/mp.17653

Medical Physics, 52, 4, pp. 2581-2592, 2025-02-04

Received: 30 May 2024 | Revised: 11 January 2025 | Accepted: 15 January 2025

DOI: 10.1002/mp.17653

RESEARCH ARTICLE

MEDICAL PHYSICS

Electron beam monitoring of a modified conventional medical accelerator with a portable current transformer system traceable to primary electrical standards

James Renaud[1] | **Bryan Richard Muir**[1] | **Andrew Williams**[2] | **Malcolm McEwen**[1]

[1]Metrology Research Centre, National Research Council Canada, Ottawa, Ontario, Canada

[2]Wellington Blood and Cancer Centre, Medical Physics, Wellington, New Zealand

Correspondence
J. Renaud, 1200 Montreal Rd., M-35, Ottawa, Ontario K1A 0R6, Canada.
Email: james.renaud@nrc-cnrc.gc.ca

Abstract

Background: Ultra-high dose rate radiotherapy (UHDR) delivers therapeutic doses at rates >40 Gy/s in a fraction of a second, aiming to enhance the therapeutic ratio through the FLASH effect. The substantial increase in UHDR beam current poses serious challenges for conventional active dosimeters. Integrating current transformers (ICT) offer a nondestructive solution for accurate monitoring, enabling the type of fast transient readout that will be crucial for UHDR treatment verification.

Purpose: The aim of this study is to build and characterize a clinically deployable ICT system and to develop an accurate calibration methodology for absolute charge determination that is traceable to primary electrical standards.

Methods: The ICT was constructed from a Super MuMetal® toroid, and its secondary winding was made from 50 Ω coaxial cable. A 3D-printed case with an internal conductive coating shields the toroid assembly from interference. The ICT readout involves a custom differential amplifier and a commercial flash analog-to-digital converter. The system was calibrated using a bespoke sub-μs current pulser in the range of (2 to 16) mA, which itself is traceable to electrical standards via an in-house built electrometer with a calibrated feedback capacitor. The performance of the ICT was evaluated as a milliampere-scale beam monitor against concurrent absorbed dose graphite calorimetry irradiation measurements acquired on a specially tuned medical accelerator for UHDR delivery.

Results: The ICT responses for nominal test pulses, generated by a function generator and a current pulser, exhibited accurate reproduction of rise and fall times within the 1 ns sampling frequency. A systematic droop effect of 0.6(1)%/μs was observed but is accounted for through the calibration chain. The calibration of the current pulser exhibited a repeatability typically better than 0.05%, with a slowly-varying leakage that can be subtracted using a linear regression of the leakage current. The ICT charge calibration demonstrated a repeatability in the range of (0.5 to < 0.05)% for charge per pulse values in the range of (0.5 to 50) nC, respectively. The ICT response showed a strong linear relationship (adj-R^2 = 0.99997) to charge per pulse. The in-beam comparison with a graphite calorimeter demonstrated the effectiveness of the ICT as an online beam monitor, independent of pulse repetition frequency in the range of (25 to 200) Hz, reducing the mean excess (i.e., independent of accelerator output) calorimeter variation to 0.3% (0.1% standard error on the mean).

Conclusions: This work demonstrates the feasibility of accurately calibrating the ICT in terms of absolute charge and applying it as a clinically deployable monitoring system of mA-scale electron beams delivered by a medical accelerator.

KEYWORDS
beam current monitor, calorimetry, current transformer, FLASH, UHDR

1 | INTRODUCTION

Ultra-high dose rate radiotherapy (UHDR) represents a novel, as-of-yet largely preclinical, approach to treatment involving the administration of therapeutic-level doses at rates typically exceeding 40 Gy/s in well under a second. The radiobiological impetus for this approach is an enhancement of the therapeutic ratio through increased healthy tissue sparing, the so-called FLASH effect, though the specifics of the mechanism and the conditions needed to achieve it are not well understood.[1] The FLASH effect has been observed for several radiation types, including megaelectronvolt electrons, hadrons, orthovoltage x-rays, and most recently, millivolt photons.[2–4] For most pulsed UHDR electron beams, the dose rate gain is due to an increase in the pulse current (∼mA) by roughly three orders of magnitude relative to conventional radiotherapy (∼μA). While this amplified charge-per-pulse is nothing novel for industrial irradiators,[5] it does pose new metrological challenges in the more stringent clinical context. The performance of many commonly used conventional therapy dosimeters, such as air-filled ionization chambers (ICs), solid-state detectors, and scintillators, suffer under UHDR irradiation conditions through some combination of reduced ion collection efficiency, quenching, and radiation-induced material degradation.[6,7] The influence on ICs is particularly problematic, since in addition to being relied upon for clinical reference dosimetry, they also form the basis of beam monitoring in most medical accelerators. Prohibitive ion recombination render ICs currently unsuitable for accurate monitoring in UHDR beams, necessitating the investigation of alternative approaches.

Integrating current transformers (ICT) have been shown to provide accurate, nondestructive monitoring of absolute fluence, and thus absorbed dose, of UHDR electron beams on a pulse-by-pulse basis and have been used by National Metrology Institutes (NMIs) for decades.[8] For UHDR experiments involving research accelerators[9] and specialized irradiators,[10–13] ICTs have proven reliable in situations in which conventional transmission ICs are unsuitable. The added advantage of current transformer-based beam monitoring is the potential for fast (ns-scale) transient readout of the output, permitting accurate quantification of the pulse structure and frequency. This is particularly attractive as a means of independent delivery record and verification, considering that the timescale of UHDR treatments will likely not allow for active control of the beam.

To our knowledge, the use of ICTs as UHDR electron beam monitors has been constrained to commercial models that are not traceable to primary standards, have not been designed for external use on a medical accelerator in general, and tend to have response times >100 ns. Response time is of fundamental importance to time-domain measurements, since it is one of the parameters that dictates the fidelity of the recorded signal. Given that the structure of an electron pulse is generally faster than 100 ns, and that the irradiation conditions needed to achieve the FLASH effect are not yet well understood, it follows that the ability to more faithfully record the temporal structure of each pulse is desirable. Furthermore, ICT application to conventional (i.e., C-arm) medical accelerators, the sole UHDR option to researchers that do not possess a dedicated irradiator, has, to the best of our knowledge, yet to be reported. The aim of this work is two-fold: (i) to build a fast (rise/fall times ∼10 ns) and clinically deployable ICT system from the ground-up with a calibration traceable to primary electrical standards, and (ii) to assess its performance as an online monitor of high-energy electrons provided by a conventional accelerator tuned to produce milliampere-scale electron beams. Traceability is sought as it offers greater dose standardization across institutions, as well as the means to verify Monte Carlo dose-per-incident electron calculations. The performance of the ICT system is evaluated directly against calorimetry-based absolute dose measurements, which have been shown to provide the highest achievable level of dosimetric accuracy in UHDR beams.[14,15]

2 | METHODS

2.1 | Current transformer design

The key components of the ICT system presented in this work are depicted schematically in Figure 1 and shown in Figure 2. The transformer toroid under investigation is classified as a type 13c, constructed using a 0.05 mm SM2 Ni-Fe alloy supermumetal tape (Telcon Ltd., Crawley, UK). The toroid's external diameter measures 159 mm, while the internal diameter is 114 mm, and the axial length extends to 25.4 mm. The toroid is encased in a phenolic resin plastic containing silicone

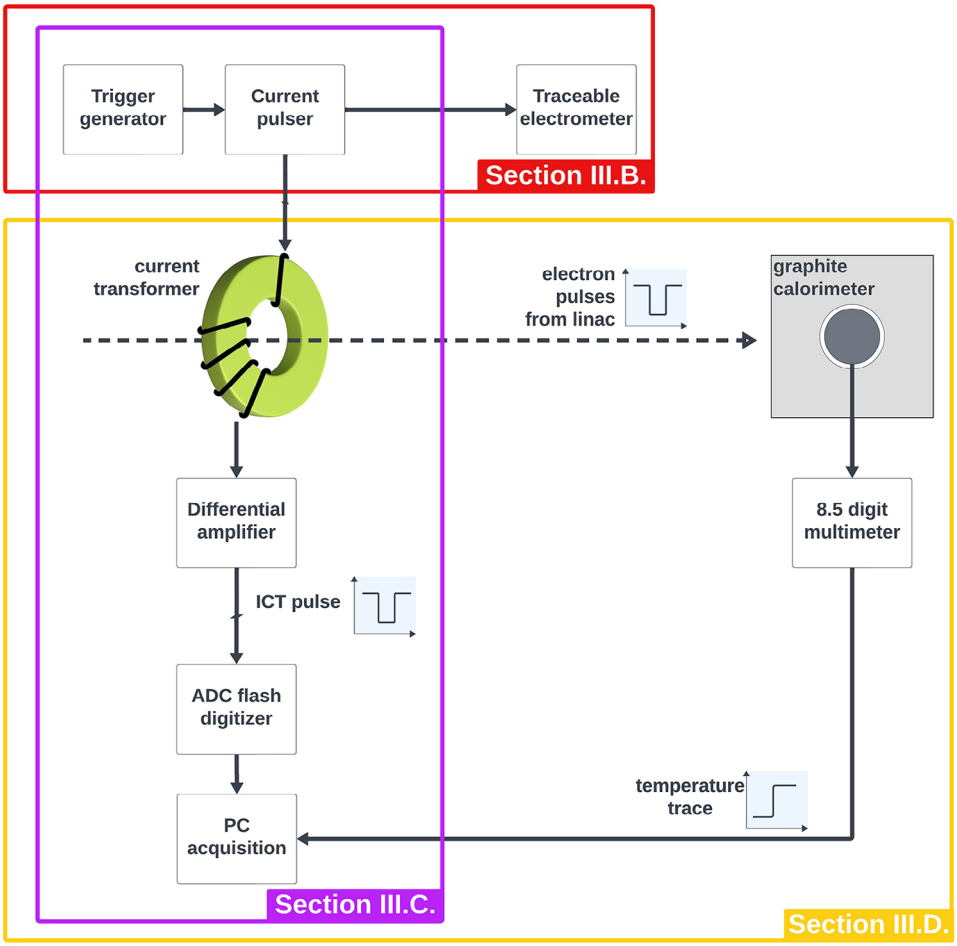

FIGURE 1 The key components of the ICT system and their relevant Results sections. Bounded in red, violet, and mustard, respectively: (i) Section 3.2., electrical calibration of the current pulser in terms of charge per pulse, (ii) Section 3.3., electrical calibration of the current transformer system in terms of charge per pulse, and (iii) Section 3.4., direct comparison of current transformer system and graphite calorimetry responses to electron beam irradiation. ICT, integrating current transformers.

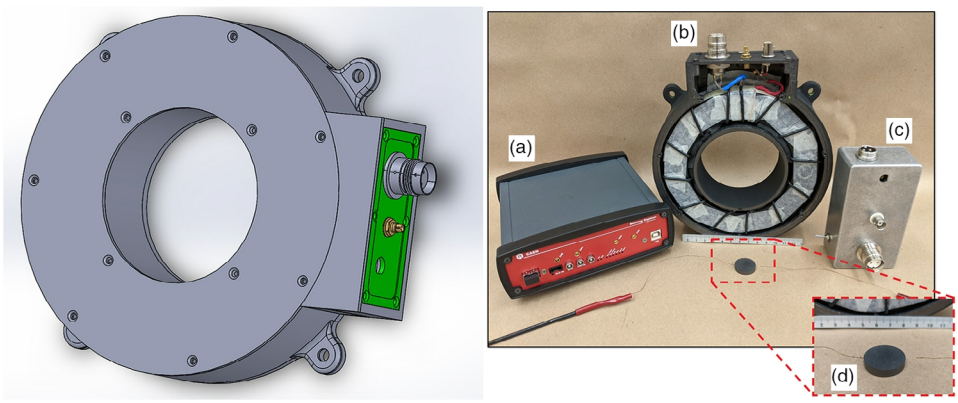

FIGURE 2 *(left)*—A model of the 3D-printed beam current transformer case with 9-cm bore that was fabricated with a μm-thin internal conductive coating of graphite. The case has four mounting points and is electrically isolated from the grounding of the accelerator. (*right*)—The key components of the ICT system (a) 12-bit 1 GHz analog-to-digital converter (ADC); (b) current transformer in 3D-printed case; (c) differential amplifier, (d—zoomed in) GCAL core. GCAL, graphite calorimeter; ICT, integrating current transformers.

grease to form an antivibration cushion. The secondary winding was wound around the outer surface of the plastic casing using RG174 50 Ω coaxial cable. Two identical lengths of the cable are interconnected by symmetrically cross-connecting the braid and center conductor.[16]

Six evenly-spaced turns were precisely wound in opposite directions until they converged diametrically opposite the crossover point. At this intersection point, the two shields were interconnected. The two center conductors were wound and extended from the toroid to be soldered onto a twin axial bulkhead connector. This winding arrangement is equivalent to 24 turns of normal wire, considering both the shield and center core of the coaxial cable.

The choice of using 50 Ω coaxial cable for the secondary winding, instead of conventional wire, serves two purposes. First, the described winding technique is intended to eliminate electrical field effects. Second, this winding configuration results in an output impedance of 100 Ω. Consequently, the secondary winding can be directly connected to a 100 Ω twisted pair coaxial cable for transmitting the output pulse to the electronics in the accelerator bunker, located well out of field.

To optimize the signal-to-noise ratio (SNR) of the ICT output, a 3D-printed polylactic acid casing was devised and fabricated with a μm-thin internal conductive coating of graphite (DAG 154, Acheson Colloids Canada Limited, Brantford, Canada). This casing has a 9-cm bore, four holes around the outside to accommodate fastening, and is electrically isolated from the grounding of the accelerator, which tends to be noisier than the mains ground. The toroid's signal outputs from the casing through a 100 Ω twin-axial cable connector, which is connected to the cable carrying the pulse to a differential amplifier (see Section 2.2). Additionally, there is a 50 Ω coaxial cable connector on the toroid casing for introducing a calibration pulse (see Section 2.3).

2.2 | ICT readout and signal processing

After traveling along the connecting cable from the ICT, the output signal undergoes termination through a 50 Ω metal film resistor on each signal line. The positive and negative pulses from the toroid typically accumulate some noise during the 6 m cable run. Nevertheless, the majority of this noise can be eliminated by employing a differential amplifier to subtract one signal from the other.

The op-amps at the heart of the differential amplifier, as shown in Figure 3, are Texas Instruments type OPA847 and type OPA842, a combination providing a user-selectable nominal output gain of 5 or 43. The low gain setting was used throughout this study due to favorable SNR. A stepped-down mains supply provides the op-amps with the necessary ±5 volts of direct current (VDC) via a rectifier and 78L10 voltage regulator. All resistors in the build are high-precision metal film. To minimize the possibility of the amplifier oscillating at high frequencies, a printed circuit board was conceived and carefully assembled. The input stage of the amplifier on both sides of the circuit board was designed to be as symmetrical as possible.

The circuit board also serves the purpose of providing a copper ground plane. An effective ground reduces stray signal pickup, serves as a low-resistance, low-inductance common return path for both signal and power, and facilitates heat dissipation from the active circuit package pins into the surrounding air through convection.

The output of the differential amplifier is fed via a short (∼0.3 m) coaxial cable to be digitized by a flash analog-to-digital converter with 10-bit resolution, 1 $V_{peak\text{-}to\text{-}peak}$ input dynamic range, and a sampling rate of 1 GS/s (DT5751, CAEN S.p.A., Italy). Analogous to a digital oscilloscope, the digitizer can capture microsecond-scale waveforms at a rate in excess of 1 kHz, which is more than sufficient for the highest accelerator repetition rates. Each trigger-inducing waveform is recorded as an individual event in a larger SQLite3 binary file (e.g., a single irradiation comprising of many beam pulses) using the manufacturer-provided acquisition software (CAENScope rev. 1.3, CAEN S.p.A., Italy). Most (>99%) of the signal that occurs between pulses is not recorded. The communication to and from the digitizer is provided through USB.

A signal processing script was written in Python (Spyder IDE v5.4.3, Python v3.11.4) to decode the acquired waveforms from byte format to floating point. The script also extracts the digitizer settings used during the acquisition (e.g., channel number, dynamic range limits, etc.). Every event has a common duration and time point at which the trigger level was met. An example of a ∼4 μs ICT output waveform in response to a ∼2 μs accelerator beam pulse is shown in Figure 4. The signal processing approach was kept relatively straightforward: A mean baseline signal is first determined by averaging over a given number of initial samples, in this study the pre-trigger period was divided into two (corresponding roughly to the first 0.5 μs in Figure 4), and subsequently subtracted from the waveform. The waveform is then integrated over a range that is initially defined by a signal threshold set to be slightly greater than the baseline variation and then symmetrically expanded by 10%. A larger than necessary time range is not desirable because the SNR would only decrease. This is because the net signal from the ICT over a long enough timeframe approaches zero (i.e., direct current (DC) components of the primary are not transformed).

2.3 | Charge calibration chain

The calibration circuit is based on a single winding of insulated wire with a diameter of 0.5 mm, wrapped around the toroid and connected to a 50 Ω metal film resistor to minimize impedance mismatch with the cable.

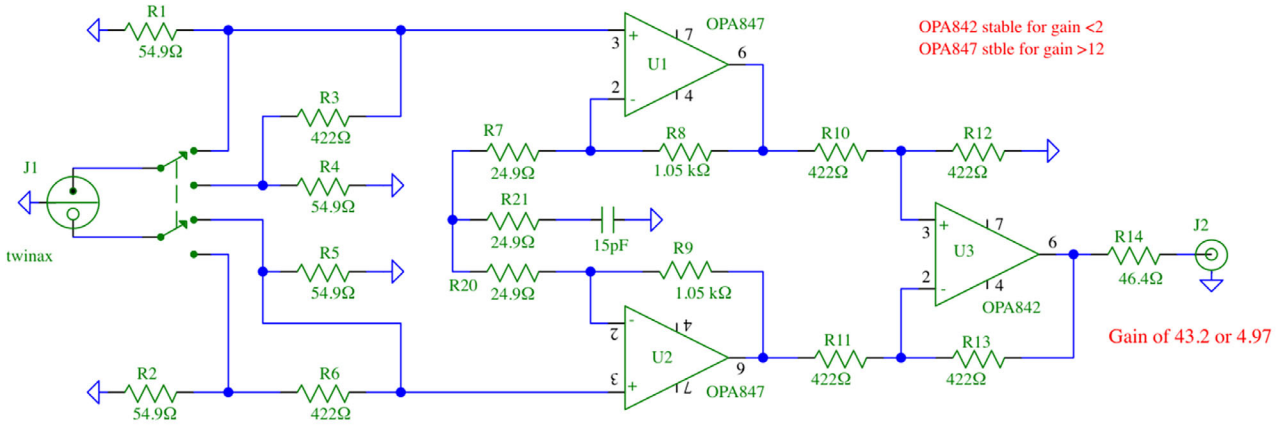

FIGURE 3 A circuit diagram of the differential amplifier circuit board that is used to minimize common mode noise picked up by the twin axial cable leading from the current transformer. The circuit components, include the high-precision metal film resistors, are arranged as symmetrically as possible. The op-amps are Texas instruments type OPA847 and type OPA842, a combination providing a user-selectable nominal output gain of 5 or 43.

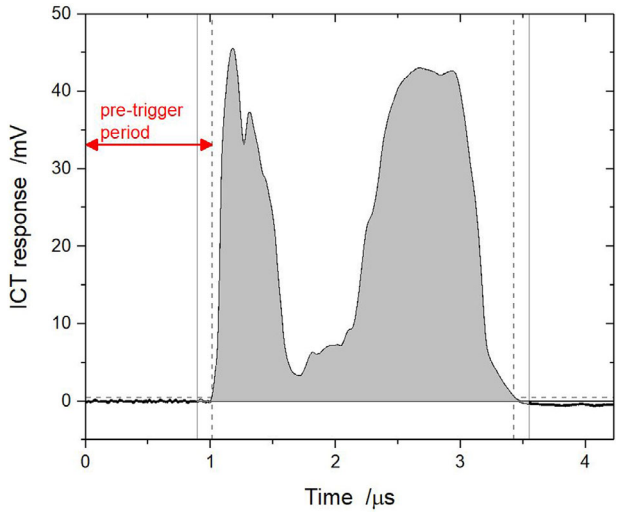

FIGURE 4 An example of a waveform originating from the ICT in response to a nominal 2 μs electron beam pulse. Signal processing of a waveform consists of subtracting the mean baseline as determined over the first half of the pre-trigger period, and then integrating the resulting signal over a range defined by signal thresholds met on the initial rise and final fall of the pulse (depicted by the shaded region of the curve bound by the vertical dashed lines). ICT, integrating current transformers.

This arrangement allows the application of a known current pulse to establish the absolute charge calibration and confirm the stability of the ICT system. This verification can be conducted in situ without disassembling the setup from the accelerator.

Designed and constructed at the National Physical Laboratory (NPL, the UK's NMI), a precision charge pulser was employed to mimic an accelerator electron beam pulse.[17] The high-precision pulser was initially based on a circuit by Dunn, with subsequent modifications by National Research Council (NRC, Canada's NMI) researchers, Williams et al.[8] Adjustments to the design were made at NPL to allow the selection of pulsed currents ranging from (2 to 62) mA in 2 mA increments, and nominal pulse widths of (0.1, 0.2, 0.5, 1, 2, and 3) μs to best represent the available accelerator pulse widths at the time. The device is externally triggered by a +6.6 V edge; in our setup, this is provided by a BNC Model 645 arbitrary waveform generator (Berkeley Nucleonics Corp., USA) operated in a configurable ''burst mode" (i.e., a successive train of N pulses). The pulser can also be operated in a constant (non-pulsed) current mode.

Commercially available electrometers used in radiotherapy often do not permit input currents on the order of mA without some form of signal conditioning. Therefore, the current pulser is calibrated in terms of charge-per-pulse using a simplified in-house made electrometer derived from the NPL design described by Sanders.[18] A Philips type-341 0.47 μF polycarbonate capacitor with a calibration traceable to national electrical standards is used as the feedback component in the electrometer circuitry. The amplification circuit consists of the highly specialized Analog Devices type 310J op-amp, chosen for its extremely low input bias current. The 310J serves as a buffer between the high-resistance source and low-resistance measuring circuit.

The current pulser is connected to the electrometer's input using a coaxial cable, triggered by the BNC 645 to pulse N times, and the voltage produced across the feedback capacitor of the electrometer is then measured using an HP3548A 8.5 digit multimeter (Hewlett-Packard, USA) and analyzed graphically using a LabVIEW (v2015, National Instruments, USA) routine developed in-house. The number of pulses, N, and the pulse repetition frequency (PRF) are chosen to be similar to the realistic accelerator deliveries. The charge per pulse, Q_{pulse}, can then be determined with

$$Q_{pulse} = \frac{\Delta V_{corr} \cdot C}{N} \quad (1)$$

where ΔV_{corr} is the measured change in voltage, corrected for leakage, and C is the capacitance of the

feedback capacitor. Once the voltage response of the monitor as a function of charge per pulse is established, the charge of an arbitrary radiation pulse can be determined within the current-time product limits of calibration.

2.4 | Absorbed dose graphite calorimetry

In this study, a graphite calorimeter (GCAL) is used as the ground truth when directly comparing against the relative response of the ICT under irradiation (see Section 2.6), since it has been previously shown that these types of dosimeters are uninfluenced by dose-per-pulse up to at least several grayscale per pulse.[14,15] Calorimeters serve as the fundamental foundation for primary absorbed dose standards in several countries, functioning based on the principle that the interaction of radiation in medium results in a detectable temperature rise. Moreover, traceability of these devices can be established independent of radiation measurements in terms of electrical and/or temperature standards.[19]

During the experiments, the temperature of the GCAL was continuously measured while it was operated passively, meaning there was no active thermal regulation of the device. When subject to conventional radiotherapy fields, this approach is not feasible without a stabilized ambient environment provided by either: (i) a precisely thermally-regulated phantom, or (ii) a large amount (10s of centimeters) of thermal insulation combined with many hours of settling time. The challenge stems from calorimetry's low sensitivity; for 1 Gy of dose absorbed, a temperature rise of only ~1 mK is produced, so typically an irradiation needs to be 10s of seconds or more in duration to establish a satisfactory SNR. In this investigation, the accelerator was modified to increase its output by a factor of ~30, so an adequate signal can be detected by the GCAL in a matter of seconds. With this configuration, the required surrounding expanded polystyrene insulation can be substantially reduced to only a few centimeter.

The GCAL consists of a single disc of graphite (referred to herein as the core), 21.6 mm in diameter and 4.4 mm thick. Two diametrically opposed 0.5 mm holes, each 8 mm deep were drilled in the core to accommodate each a thermistor (i.e., temperature-sensitive resistors) (Micro-BetaCHIP, TE Connectivity, USA) with a nominal resistance of 10 kΩ and a per-degree sensitivity of 4% at 25°C. Temperature calibration of the thermistors was performed according to a procedure previously reported that has an associated type B uncertainty of 0.05%.[20] Under irradiation, the GCAL measures the mean absorbed dose in the core, D_{core}, based on its relation to the temperature rise, ΔT, and the specific heat capacity of the core, $c_{p,\text{core}}$, with

$$D_{\text{core}} = c_{p,\text{core}}\ (T) \cdot \Delta T \cdot \prod k_i \tag{2}$$

For the relative comparison against the ICT, the product of the correction factors, k_i, which normally includes heat transfer, heat defect, radiation field perturbation, and dose nonuniformity, can be assumed to be unity, since none of the factors vary appreciably as measurements are repeated within a given setup. The combined thermistor resistance is logged with an HP3548A 8.5 digit multimeter and analyzed by extrapolating the pre- and post-fit signals to the midpoint of the irradiation, a method typical for absorbed dose calorimetry.[20] In this study, absolute dose rates are not reported since, (i) they are largely inconsequential to the objective of testing the performance of the monitoring system in a milliampere-scale electron beam, and (ii) because these would be based on uncorrected calorimeter readings (e.g., no heat transfer correction, dose-to-water conversion factor, etc.). The calorimeter simply provides a dose rate independent reading that can be compared in relative terms against the monitor chamber.

2.5 | Converted medical accelerator

Experiments were performed using an Elekta Synergy linear accelerator (Elekta AB, Sweden) equipped with an Agility collimator and a commercially available high dose rate electron (HDRE) module. When enabled, the HDRE mode of operation sees the electron current output increased by an order of magnitude compared to conventional mode (e.g., from ~0.05 to ~0.5 Gy/s under reference conditions). Clinically, the HDRE module serves to attenuate the monitor chamber signals by a factor of 10 before reaching the dosimetry system, effectively preventing software interrupts. The working principle of HDRE mode was extended by adding an additional array of current dividers, as described by Snyder et al., between the existing module and the dosimetry system to further increase the permissible electron beam current and produce UHDR conditions.[21] The 8 MeV electron beam was then manually tuned by adjusting the gun filament currents and magnetron settings towards those used during photon delivery. Bending magnet currents had to also be changed to compensate for the additional beam intensity traveling along the slalom (i.e., the achromatic magnetic deflection system used in Elekta accelerators). Furthermore, the primary scattering foil was set to its open position, and an open slot in the secondary scattering carousel was selected. Tuning of the beam had no impact on the pulse width, which remained nominally 2 μs wide. Signals acquired from the toroid, a direct measure of the time dependent electron fluence, served

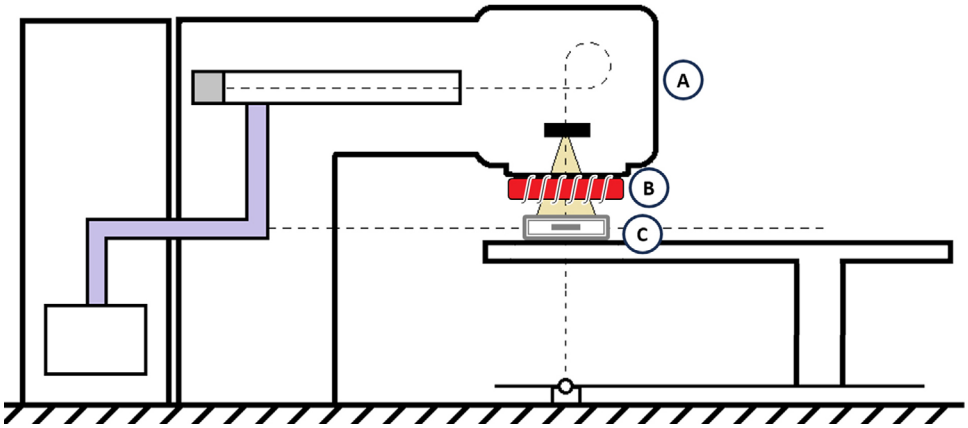

FIGURE 5 A schematic of the experimental setup used in the direct relative comparison of the ICT and GCAL. (a) A medical c-arm linear accelerator producing a custom-tuned 8 MeV electron beam with a pulsed current of roughly 16 mA and maximum repetition rate of 200 Hz. (b) The ICT was fastened to a steel and acrylic collimating plate assembly, which was in turn externally mounted to the head of the accelerator centered over the beam exit window. (c) The expanded polystyrene block containing the calorimeter and a 5 mm layer of water-equivalent plastic were positioned at an SSD of 100 cm along the beam central axis. GCAL, graphite calorimeter; ICT, integrating current transformers; SSD, source to surface distance.

as real-time visual feedback while tuning the beam. Tuning was completed when the response of the toroid peaked around (40–45) mV, which is approximately equivalent to a primary beam current of 6 mA (see Section 3.3). At the highest PRF setting (200 Hz) with this tuning, the absorbed dose rate to graphite was about 32 Gy/s (roughly equivalent to 40 Gy/s or 0.2 Gy/pulse in water) at a source to surface distance (SSD) of 100 cm (this would scale to approximately 1 Gy/pulse at an SSD of 45 cm). While adequately precise for the purposes of this work, the absolute dose values provided in this work are based solely on the product of the measured temperature rise and the specific heat capacity, and do not consider heat transfer or any other corrections typically required for calorimetry. As such, stated dose values are meant to be illustrative and are expected to have associated corrections on the order of 10%.

2.6 | Direct relative comparison of ICT and calorimeter

The ICT was fastened to a (320×320) mm^2 collimating plate assembly consisting of a 12 mm intermediate layer of acrylic and a 15 mm thick layer of stainless steel, both having a 9 cm diameter hole at their centers. The steel plate was externally mounted to the head of the accelerator centered over the beam exit window with the toroid positioned downstream and the gantry angle set to 0°. The expanded polystyrene block containing the GCAL and a 5 mm layer of water-equivalent plastic (Virtual Water, Med-Cal) were positioned at an SSD of 100 cm along the beam central axis (Figure 5).

Each acquired measurement set consisted of 10 consecutive irradiations of the modified 8 MeV electron beam for a nominal duration of 45 s. The relatively long irradiation period was chosen to accommodate the analysis of the calorimetry data, which was performed to be consistent with primary standard techniques. Likewise, sets of 10 repeated calorimetry measurements is expected to produce type A uncertainties of less than 0.2%.[20] Initiation and termination of the deliveries was accomplished in terms of monitor units (MU; 29, 57, 115, and 230), which were selected to maintain a consistent delivery time across different PRF setting (25, 50, 100, 200) Hz, respectively. MUs were used to terminate the beam as it required no modification to the accelerator control software, and alternative means based on pulse counting were not required, though it may have improved the timing consistency. Nevertheless, a delivery time consistent to within 1 s is more than adequate to consider calorimetry-related heat transfer effects as being constant. For every run, the ratio of the dose absorbed in the GCAL and the integrated pulse from the ICT was determined. For each measurement set, the relative variations of the ratios were tracked as a measure of the accuracy of the ICT as a beam monitor. The level of consistency observed in the GCAL to ICT ratio indicates the sensitivity of the ICT response to variations in electron fluence that concurrently influences the calorimeter measurement downstream. While the GCAL to ICT ratio is not inherently representative of the fidelity of the ICT signal, a faster response time will in principle capture signal variations on a shorter timescale.

3 | RESULTS

3.1 | Output pulse shape

Figure 6 shows the toroid responses for two instances of nominal 3 μs test pulses with rise and fall times of (15–20) ns (defined between 10% and 90% of the maximum), one being the 1 V square wave output of a BNC

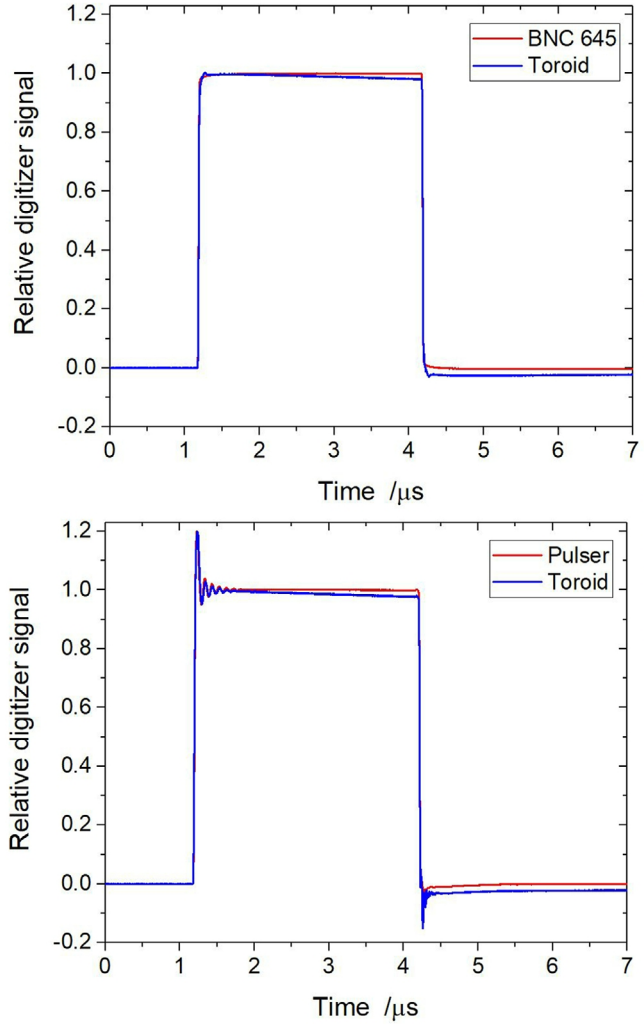

FIGURE 6 The relative output signals of the current transformer in response to 3 μs test pulses in the form of a (*top*) 1 V square wave from a BNC 645 function generator, and (*bottom*) the 16 mA setting of the current pulser. All plots have been normalized by extrapolating the plateaus back to the time point that intersects with the rising edges of the pulses.

645 function generator, the other being the 16 mA setting of the current pulser. In both cases, the output of the current transformer reproduces the rise and fall times to within the sampling frequency of 1 ns. A fractional droop of 0.6(1)% per microsecond was measured at the end of both toroid output pulses, an effect that is clearly identified by the overshoot past the baseline on the falling side of the pulses. Although the consequence of droop is a systematic underestimate in Q_{pulse}, this is effectively accounted for through the calibration chain presented in Section 2.3. The relative variation of the baselines, defined as the standard deviation of 500 samples immediately preceding the pulse, of the current pulser and corresponding transformer response was determined to be 0.01% and 0.03% (nominally equivalent to 2 and 5 μA), respectively. This measure of the baseline is representative of when the accelerator is in standby mode (or, for instance, the toroid is being

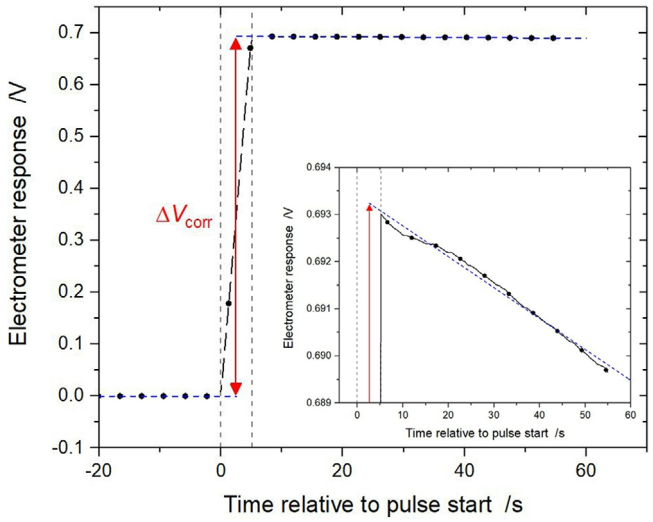

FIGURE 7 An example of a current pulser calibration run with nominal settings of 2 mA and 1 μs as measured by the electrometer described in Section 2.3. At time $t = 0$, a series of 200 pulses were triggered at a rate of 40 Hz, the beginning and end of which are identified by the vertical dashed lines, inducing a buildup of voltage across the calibrated feedback capacitor. The depicted electrometer response has been background-subtracted. To determine the voltage rise, ΔV_{corr} (red vertical double-ended arrow), the slowly varying post-drift data is linearly extrapolated back to the midpoint of the pulsing period, as shown in the inset.

operated on the bench). Under irradiation conditions, as shown in Figure 4, the ICT baseline variation roughly doubles to 10 μA in response to the increased levels of radio frequency (RF) interference.

3.2 | Calibration of current pulser

A summary of the measured pulser output in terms of pulse width and current settings in the nominal range of (0.1 to 3) μs and (2 to 16) mA, respectively, is provided in Table 1. In constant current mode, the pulser output is observed to be consistent to within (100–200) nA across the range of settings investigated, or about (0.01–0.1)% of the nominal value. The measured pulse widths are independent of current setting to within 15 ns for pulse widths less than 1 μs, and within 25 ns for 1 μs and greater.

The leakage of the electrometer with the pulser connected but idle was measured to be 1.2(2) mV/s with a rate of variation low enough to permit accurate linear subtraction of the background for runs of up to 5 min (~2.5 min pre- and post-drift collected). Once corrected for drift, the remaining variation of the background signal is on the order of 40 μV. Figure 7 shows an example of a 200-pulse, 40 Hz calibration run with the pulser output set to 2 mA and 1 μs. This example was one of a series of 10 consecutive calibration runs, for which the mean voltage rise was determined to be 0.6929 V ± 0.06%, an equivalent Q_{pulse} of 1.6853(7)

TABLE 1 Characterization of the pulser output as a function of constant current and pulse width settings in the ranges of (2 to 16) mA and (0.1 to 3) μs, respectively.

Current setting (mA)	Measured DC current (mA)	FWHM measured for pulse width setting (us)					
		0.1	0.2	0.5	1	2	3
2	1.7453	0.141	0.240	0.516	1.043	2.018	2.996
4	3.6632	0.143	0.249	0.523	1.057	2.031	3.009
6	5.6161	0.146	0.250	0.525	1.061	2.036	3.015
8	7.6111	0.147	0.250	0.526	1.064	2.039	3.017
10	9.6133	0.147	0.250	0.527	1.066	2.040	3.019
12	11.6179	0.147	0.249	0.529	1.067	2.041	3.019
14	13.6226	0.147	0.248	0.529	1.068	2.042	3.020
16	15.7521	0.147	0.247	0.529	1.068	2.042	3.021

Note: The current was measured directly with an HP3458A 8.5 digit DMM to a stable precision of 200 nA, while the FWHM were determined using the CAEN DT5751 digitizer to within the sampling frequency of 1 ns.
Abbreviation: FWHM, full widths at half max.

nC. In general, the repeatability (i.e., sample standard deviation) of this method was typically better than 0.05%, but for $Q_{pulse} < 1$ nC, this approached 0.1%. The measured Q_{pulse} was found to be independent of PRF and number of pulses within the investigated range of (40 to 400) Hz and N = (100 to 200). In general, the sampling statistics favor the greatest number of pulses (increased signal) delivered within the shortest time (decreased uncertainty on the extrapolation).

3.3 | ICT charge calibration

The pulse calibration values obtained in the range of (4 to 16) mA were used to directly calibrate the ICT response in terms of Q_{pulse} over a range spanning nearly two orders of magnitude, ~(0.5–50) nC/pulse. For each pulser setting investigated the average ICT response to 200 current pulses is shown in Figure 8. The repeatability of the ICT response, defined as the standard deviation on the mean integrated response, ranged from 0.5% to less than 0.05% at the lowest and highest charge per pulse settings. In absolute terms, the repeatability varied between (10^{-11} and 10^{-10}) V·s, an amount that is not clearly visible with the scale shown in Figure 8. A strong linear relationship (adj-R^2 = 0.99997) between the ICT response and the amount of charge delivered per pulse was observed, with nearly all residuals lying within 1% of the regression, and more than half within 0.5%. Overall, the sensitivity of the ICT system was determined to be 6.863(5) V/A.

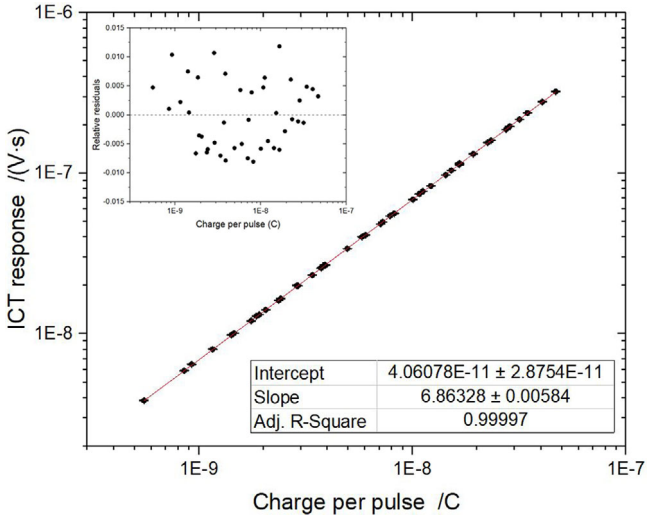

FIGURE 8 Calibration plot showing the strong linear relationship between the integrated ICT system response and the amount of charge delivered per pulse over a range of two orders of magnitude. At this scale, the uncertainty bars are not visible. The relative residuals of the linear regression are seen in the inset plot and are, in general, randomly distributed. All but three points agree within 1% of the fit (maximum deviation is 1.2%) and more than half of all points are within 0.5%. ICT, integrating current transformers.

3.4 | ICT-calorimeter in-beam comparison

As a first stage evaluation of the ICT's performance as an online beam monitor, concurrent absorbed dose and beam current measurements were carried out for the custom tuned 8 MeV electron beam. Figure 9 depicts an example GCAL acquisition for the lowest PRF investigated along with the determination of the 155 mK radiation-induced temperature rise. The repeatability (i.e., standard deviation on the mean) for the GCAL and ICT across the four PRF settings under study varied between (1.0 and 1.7)% in a highly correlated manner. The average temperature rise for the PRF settings of (25, 50, 100, 200) Hz were (155, 297, 605, 1147) mK with an associated sample standard deviation of (1.0, 1.7, 1.4, 1.5)%, respectively. Since the temperature rise and absorbed dose are directly proportional, the sample standard deviations also apply to the determination of

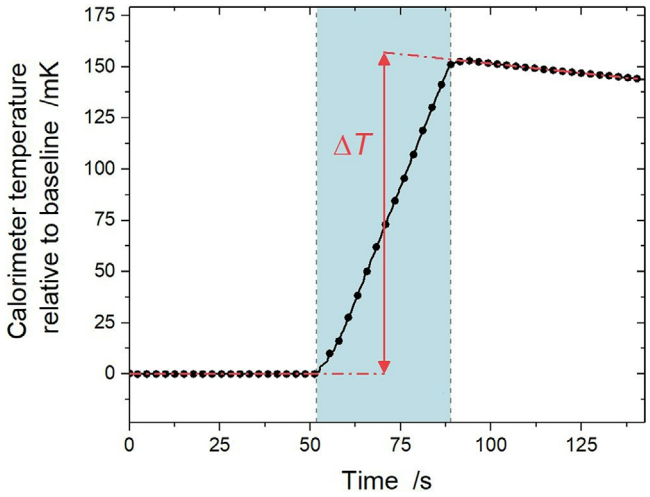

FIGURE 9 Example of a baseline-corrected GCAL run acquired at a nominal repetition rate of 50 MU/min (PRF of 25 Hz). A radiation-induced temperature rise of 155 mK was measured, which corresponds to an absorbed dose to graphite of about 110 Gy. An extrapolation of the post-drift data to the midpoint of the irradiation period (shaded region) is performed to determine the heat loss-compensated temperature rise. GCAL, graphite calorimeter.

dose. In contrast, the MU values reported by the accelerator control software postirradiation exhibited almost no variation (consistent within 0.1% for a given delivery configuration). Normalizing the GCAL response to the ICT response reduced the excess variation (i.e., not due to accelerator output) to 0.3% on average with an associated 0.1%standard error on the mean. Furthermore, the choice of PRF was seen to have no influence on the GCAL to ICT ratio, yielding a mean value of 1.328(4) cGy/nC with an associated 0.3% standard deviation.

3.5 | Uncertainties

For the pulser calibration, type A uncertainty ranges from (0.1 to 0.01)% ($k = 1$) for Q_{pulse} values between (0.5 to 50) nC, respectively. The type B uncertainty associated with the feedback capacitor calibration is 0.0001% with a coverage factor of $k = 2$, and thus can be considered negligible. Additional systematic effects include the small additional capacitance contributions from wiring the circuit (e.g., wires/solder joints/connector), as well as temperature effects on the electrometer response, neither of which have been characterized in this study. Similarly for the ICT calibration, sampling uncertainty was dependent on the magnitude of delivered Q_{pulse}, with standard deviations that varied between (0.05 and 0.5)% ($k = 1$) for charges in the range of (50 to 0.5) nC. The calculated intercept of the regression in Figure 8 ($4(3) \times 10^{-11}$ V·s) suggests the presence of a small (~0.001 to 0.1)% but statistically significant systematic effect. During irradiation, Q_{pulse} from the ICT was determined with an associated type A uncertainty of 0.25% for all PRFs. The excess variation observed in the GCAL to ICT ratio points to additional type A uncertainty on the order of (0.05–0.15)%, which is generally consistent with accelerator-based calorimetry, though it is unclear what proportion is contributed by each detector. Variation in the GCAL heat transfer is an unlikely source, as no run-to-run trending in the GCAL-ICT ratio was observed.

4 | DISCUSSION

The results of the irradiation experiments suggest that the performance of the ICT as a nondestructive beam monitor for this 6 mA electron beam is on par with that of traditional transmission ICs used in conventional radiotherapy treatments. The level of repeatability achieved for the GCAL-ICT ratio (0.3%) is consistent with primary standard water calorimeter measurements performed on medical accelerators with auxiliary IC-based monitoring at the NRC.[22]

The level of precision of the ICT is anticipated to further improve as the delivered current per pulse is increased, as was observed with the charge calibration procedure using the current pulser. Since the repeatability was measured to be ~0.5% at 4 mA and better than 0.05% at 16 mA, the ICT can effectively be used to measure as few as $N = (1–5)$ pulses, as is anticipated for ultra high dose rate radiation therapy (UHDR RT), with an associated uncertainty comparable to ion chambers in conventional beams. In comparison to other ICT-based beam monitoring studies employing commercial transformers,[8–12] the rise and fall times measured in this work are about an order of magnitude faster (< 15 ns), which means that even the narrowest anticipated pulse structures can be resolved and pertinent pulse features, such as pulse width, can be more precisely quantified. The baseline variation of the ICT signal during irradiation was determined to be on the order of 10 μA, which is a good estimate of the lower detectable current limit, though the type A uncertainty will be strongly dependent on the total charge per pulse. This places conventional electron beam and UHDR hadron therapy monitoring well out of reach, with an associated low-end requirement of ~100 nA. In principle, it would be feasible to monitor conventional electron therapy if the pulse width was reduced to a few 10s of nanoseconds, thus boosting the peak current to meet the minimum detectable limit of the ICT. The sensitivity of the monitor's response was determined to be 6.863(5) V/A, so for this particular set of electronics, an upper detectable current limit is dictated by the dynamic range of the digitizer (1 V); about 145 mA. Digitizers with a 10 V dynamic range are common, so it is expected that the requirements of any UHDR irradiator could be met with this monitoring system.

The modest fractional droop of 0.6%/μs means that the acquired signal is a high-fidelity representation of the primary intensity and is generally on par

with commercially available alternatives.[23] The built-in calibration loop is comparable to the Q-loop wire,[8] or preinstalled calibration winding, supplied by some manufacturers,[24] and offers a direct path to establish absolute charge traceability. Previous studies have clearly shown that the position of the calibration loop, or equivalent Q-loops, relative to the transformer axis has little (~0.01%) influence on the ICT response, hence no considerable dependence upon the cross-sectional electron fluence distribution is expected.[8,9] At present, no primary absorbed dose standard has been established for UHDR electrons, though accurate absolute monitoring of the beam under a fixed set of reference conditions will be a prerequisite in doing so. This ICT system is clinically deployable, easily transportable from one institution to another, and is vendor-independent. In this study, the absorbed dose to graphite per incident charge was determined to be 1.328(4) cGy/nC for all repetition rates for this particular setup. In a vacuum, this value is meaningless, but it does demonstrate how traceable monitoring can lead to improved UHDR dose standardization across institutions, potentially impacting the quality of clinical trials and patient care alike. Very few current transformer monitors are traceable to primary standards or have the capability of being externally-mounted and calibrated in-situ, and for the few that are, a complex Faraday cup is relied on to provide a measure of absolute charge at some position downstream. Being independent of the irradiator, this ICT system could be used to independently validate electron fluence and pulse structures across facilities, a potentially useful feature in which inconsistencies in delivery cause discrepancies in radiobiological studies.

Though many groups,[9–13] including this work, have shown to varying degrees of accuracy the linearity of ICT response to Q_{pulse}, it is also important to acknowledge the limitations of the technology, namely its sensitivity to backscattered charge and external electromagnetic fields. The consequence of the former is an inherent dependence on field size, SSD, and the geometry of the setup positioned downstream from the ICT, though a recent Monte Carlo-based study of (6 and 9) MeV UHDR electrons has suggested that this may play a smaller role than previously thought.[11,24] Instead, it was found that the electrical conductivity of the irradiated medium had a more substantial influence on ICT response, though the effect could be effectively mitigated through the adoption of Faraday shielding surrounding the monitor. Furthermore, the current transformer is intended to be a nondestructive beam monitor (i.e., producing no radiation field perturbation), therefore, its collimator-defined field size limit is the size of the interior bore of the casing within which the radiation transits (9-cm diameter at the exit window). Practically, larger field sizes will not only be severely perturbed by the high-Z material contained within the toroid but will have distal components of the fluence contributing nothing to the transformer response.

5 | CONCLUSIONS

The performance of an ICT capable of measuring individual mA-scale electron beam pulses from a conventional medical accelerator operating at up to 200 Hz was characterized in this work. The output response is relatively free of RF interference, has a ns-scale rise and fall time, and when used in combination with a bespoke current pulser, can be accurately calibrated in terms of absolute charge in situ. Overall, charges per pulse from irradiations were determined with a $k = 1$ type A uncertainty of 0.25%. A direct comparison of the ICT and GCAL points to the effectiveness of using such a system as an online monitor of UHDR electron beams, which will prove essential in the development of UHDR absorbed dose standards.

ACKNOWLEDGMENTS

The authors are grateful to Stewart Walker and Jean Dessureault of National Research Council Canada for the technical support with the current pulser, differential amplifier, and 3D printing, as well as Russell Thomas of the National Physical Laboratory, UK, for providing invaluable technical documentation pertaining to the electrometer design.

CONFLICT OF INTEREST STATEMENT

The authors declare no conflicts of interest.

REFERENCES

1. Vozenin MC, Bourhis J, Durante M. Towards clinical translation of FLASH radiotherapy. *Nat Rev Clin Oncol*. 2022;19(12):791-803.
2. Montay-Gruel P, Bouchet A, Jaccard M, et al. X-rays can trigger the FLASH effect: ultra-high dose-rate synchrotron light source prevents normal brain injury after whole brain irradiation in mice. *Radiother Oncol*. 2018;129(3):582-588.
3. Gao F, Yang Y, Zhu H, et al. First demonstration of the FLASH effect with ultrahigh dose rate high-energy X-rays. *Radiother Oncol*. 2022;166:44-50.
4. Schulte R, Johnstone C, Boucher S, et al. Transformative technology for FLASH radiation therapy. *Appl Sci*. 2023;13(8):5021.
5. Kutsaev SV, Agustsson R, Arodzero A, et al. Linear accelerator for security, industrial and medical applications with rapid beam parameter variation. *Radiat Phys Chem*. 2021;183:109398.
6. Subiel A, Moskvin V, Welsh GH, et al. Challenges of dosimetry of ultra-short pulsed very high energy electron beams. *Physica Med*. 2017;42:327-331.
7. Kranzer R, Poppinga D, Weidner J, et al. Ion collection efficiency of ionization chambers in ultra-high dose-per-pulse electron beams. *Med Phys*. 2021;48(2):819-830.
8. Williams AJ, McEwen MR, Burns DT. *A New Beam Current Monitor for the NPL Linear Accelerator*. NPL Report CIRM, 12. NPL; 1998.
9. Schüller A, Illemann J, Renner F, Makowski C, Kapsch RP. Traceable charge measurement of the pulses of a 27 MeV electron beam from a linear accelerator. *J Instrum*. 2017;12(03):P03003.
10. Oesterle R, Gonçalves Jorge P, Grilj V, et al. Implementation and validation of a beam-current transformer on a medical pulsed electron beam LINAC for FLASH-RT beam monitoring. *J Appl Clin Med Phys*. 2021;22(11):165-171.

11. Liu K, Palmiero A, Chopra N, et al. Dual beam-current transformer design for monitoring and reporting of electron ultra-high dose rate (FLASH) beam parameters. *J Appl Clin Med Phys*. 2023;24(2):e13891.
12. Goncalves Jorge P, Grilj V, Bourhis J, et al. Validation of an ultra-high dose rate pulsed electron beam monitoring system using a current transformer for FLASH preclinical studies. *Med Phys*. 2022;49(3):1831-1838.
13. Jain S, Cetnar A, Woollard J, et al. Pulse parameter optimizer: an efficient tool for achieving prescribed dose and dose rate with electron FLASH platforms. *Phys Med Bio*. 2023;68(19): 19NT01.
14. Bourgouin A, Schüller A, Hackel T, et al. Calorimeter for real-time dosimetry of pulsed ultra-high dose rate electron beams. *Front Phys*. 2020;8:567340.
15. Bourgouin A, Keszti F, Schönfeld AA, et al. The probe-format graphite calorimeter, Aerrow, for absolute dosimetry in ultrahigh pulse dose rate electron beams. *Med Phys*. 2022;49(10):6635-6645.
16. Sutter DF. A wide band current monitor based on pulsed transformer techniques. *IEEE Trans Nucl Sci*. 1973;20(3):665-667.
17. Dunn PC. Absolute beam charge measurements with toroid monitors: experience at the Bates Linac. *Nucl Instrum Methods*. 1979;165(2):163-167.
18. Sanders RP. *The Design and Operation of a High Quality Two-Channel Electrometer*. NPL Report RS(INT)106. NPL; 1989.
19. Renaud J, Palmans H, Sarfehnia A, Seuntjens J. Absorbed dose calorimetry. *Phys Med Biol*. 2020;65(5):05TR02.
20. Seuntjens JP, Ross CK, Klassen NV, Shortt KR. *A Status Report on the NRC Sealed Water Calorimeter*. NRC Report PIRS, 584. NRC; 1999.
21. Snyder M, Vadas J, Musselwhite J, et al. FLASH radiotherapy monitor chamber signal conditioning. *Med Phys*. 2021;48(2):791-795.
22. Muir BR, Cojocaru CD, McEwen MR, Ross CK. Electron beam water calorimetry measurements to obtain beam quality conversion factors. *Med Phys*. 2017;44(10):5433-5444.
23. Bergoz Instrumentation, Saint-Genis-Pouilly, France, www.bergoz.com
24. Pageot C, Zerouali K, Guillet D, Muir B, Renaud J, Lalonde A. The effect of electron backscatter and charge build up in media on beam current transformer signal for ultra-high dose rate (FLASH) electron beam monitoring. *Phys Med Biol*. 2024;69(10):105016.

How to cite this article: Renaud J, Muir BR, Williams A, McEwen M. Electron beam monitoring of a modified conventional medical accelerator with a portable current transformer system traceable to primary electrical standards. *Med Phys*. 2025;52:2581–2592. https://doi.org/10.1002/mp.17653